



aa/bb/cc/dd-TDI

EXPLORING COLD POOL DYNAMICS IN MONAN: INSIGHTS FROM HURRICANES

Bianca Fusinato

Master's Dissertation from the
Graduate Program in Meteorology,
supervised by Dr. Saulo R. Freitas,
approved on [day] of [month] [year].

URL of the original document:
<http://urlib.net/xx/yy>

INPE
São José dos Campos
2025

PUBLISHED BY:

Instituto Nacional de Pesquisas Espaciais - INPE
Coordenação de Ensino, Pesquisa e Extensão (COEPE)
Divisão de Biblioteca (DIBIB)
CEP 12.227-010
São José dos Campos - SP - Brasil
Tel.:(012) 3208-6923/7348
E-mail: pubtc@inpe.br

BOARD OF PUBLISHING AND PRESERVATION OF INPE INTELLECTUAL PRODUCTION - CEPII (PORTARIA Nº 176/2018/SEI-INPE):

Chairperson:

Dra. Marley Cavalcante de Lima Moscati - Coordenação-Geral de Ciências da Terra (CGCT)

Members:

Dra. Ieda Del Arco Sanches - Conselho de Pós-Graduação (CPG)

Dr. Evandro Marconi Rocco - Coordenação-Geral de Engenharia, Tecnologia e Ciência Espaciais (CGCE)

Dr. Rafael Duarte Coelho dos Santos - Coordenação-Geral de Infraestrutura e Pesquisas Aplicadas (CGIP)

Simone Angélica Del Ducca Barbedo - Divisão de Biblioteca (DIBIB)

DIGITAL LIBRARY:

Dr. Gerald Jean Francis Banon

Clayton Martins Pereira - Divisão de Biblioteca (DIBIB)

DOCUMENT REVIEW:

Simone Angélica Del Ducca Barbedo - Divisão de Biblioteca (DIBIB)

André Luis Dias Fernandes - Divisão de Biblioteca (DIBIB)

ELECTRONIC EDITING:

Ivone Martins - Divisão de Biblioteca (DIBIB)

André Luis Dias Fernandes - Divisão de Biblioteca (DIBIB)



aa/bb/cc/dd-TDI

EXPLORING COLD POOL DYNAMICS IN MONAN: INSIGHTS FROM HURRICANES

Bianca Fusinato

Master's Dissertation from the
Graduate Program in Meteorology,
supervised by Dr. Saulo R. Freitas,
approved on [day] of [month] [year].

URL of the original document:
<http://urlib.net/xx/yy>

INPE
São José dos Campos
2025

Cataloging in Publication Data

Sobrenome, Nomes.

Cutter Exploring Cold Pool Dynamics in MONAN: Insights from Hurricanes / Nome Completo do Autor1; Nome Completo do Autor2.
– São José dos Campos : INPE, 2025.
xx + 39 p. ; (aa/bb/cc/dd-TDI)

Dissertação ou Tese (Mestrado ou Doutorado em Nome do Curso) – Instituto Nacional de Pesquisas Espaciais, São José dos Campos, AAAA.

Orientador : José da Silva.

1. Palavra chave. 2. Palavra chave 3. Palavra chave. 4. Palavra chave. 5. Palavra chave I. Título.

CDU 000.000



Esta obra foi licenciada sob uma Licença Creative Commons Atribuição-NãoComercial 3.0 Não Adaptada.

This work is licensed under a Creative Commons Attribution-NonCommercial 3.0 Unported License.

Informar aqui sobre marca registrada (a modificação desta linha deve ser feita no arquivo publicacao.tex).

Informar aqui sobre fontes financiadoras (a modificação desta linha deve ser feita no arquivo publicacao.tex).

**ATENÇÃO! A FOLHA DE
APROVAÇÃO SERÁ INCLU-
IDA POSTERIORMENTE.**

Mestrado ou Doutorado em Nome do
Curso

ACKNOWLEDGEMENTS

acknowledges

ABSTRACT

Structure: GCMs and the need of parameterization, including sub-grid phenomena

Explain about the cold pools and the parameterization

Explain the dissertation's goal: explore this cold pool parameterization and select the best bulk of features to configure the CPTEC model

How are we going to do it?

Since we are working with hurricanes propagating in the ocean, we test other parameterization to take into account - How does it work?

Leave a paragraph to insert the results.

Inside Global Circulation Models (GCMs), precipitation can be modeled through cloud microphysics or convection schemes. Despite advancements in computational capabilities, computational constraints still imply the need for parameterizations for processes not explicitly resolved at the model's grid-scale.

It has been shown that to improve large-scale numerical representation it can be started by improving the sub-grid scale process representation.

Cold Pools correspond to a cold air mass descending within the downdraft. Recent studies show that cold pools are divided into two structures: the cold and dry centers and a moist ring on the edge. When it reaches the surface, it spreads out horizontally, and the high values of moist static energy on the rings combined with the gust front speed can lift the air thermodynamically and mechanically, respectively.

The spatial scale of this phenomenon is translated into sub-grid numerical representations inside the GCMs. It has been shown that cold pools can organize the formation of new convective cells, promoting their aggregation and leading to the development of mesoscale convective systems.

An investigation of the impact of the cold pool parameterization using simulations performed with the Model for Ocean-LaNd-Atmosphere PredictionN (MONAN) is proposed.

Keywords: GCM. Cold Pool. MONAN. Hurricanes. Sea Spray.

**EXPLORANDO A DINÂMICA DE *COLD POOLS* NO MONAN:
PERSPECTIVAS A PARTIR DE FURACÕES**

RESUMO

Traduzir o resumo para português

Palavras-chave:

LIST OF FIGURES

| | <u>Page</u> |
|--|-------------|
| 3.1 MPAS-A meshes and the ability to configure the meshes at different resolutions | 11 |
| 4.1 Illustration of cross-track and along-track errors. The definitions of Cross-Track Error (CTE) and Along-Track Error (ATE) are based on the distance between an observation (obs) and a forecast (fct) at the same valid time (T). This distance is computed as the great-circle distance. | 16 |
| 4.2 Workflow Overview | 20 |
| 5.1 Comparison of Storm Tracks Across All 15 Experiments | 24 |
| 5.2 Errors (distance) between the trajectories | 25 |
| 5.3 All tracks with selected experiments from Table 5.4 | 27 |

LIST OF TABLES

| | <u>Page</u> |
|--|-------------|
| 3.1 List of ERA5 Variables Used | 6 |
| 3.3 Physics bulk configuration | 10 |
| 4.1 Key Research Questions for Track, Intensity, and Rainfall Assessment . . | 13 |
| 4.3 Metrics used to evaluate rainfall forecast performance | 18 |
| 5.1 All Performed Experiments | 22 |
| 5.3 Default values for the cold pool parameterization scheme | 23 |
| 5.4 Selected Experiments | 26 |

LIST OF ABBREVIATIONS

LIST OF SYMBOLS

CONTENTS

| | <u>Page</u> |
|---|-------------|
| 1 INTRODUCTION | 1 |
| 1.1 General objective | 1 |
| 1.2 Specific objectives | 1 |
| 1.3 Scientific questions | 1 |
| 1.4 Thesis organization | 1 |
| 2 LITERATURE REVIEW | 3 |
| 2.1 Overview of convective cloud dynamics | 3 |
| 2.2 Cold pools | 3 |
| 2.3 The mass-flux approach | 3 |
| 2.4 The cold pool parameterization | 3 |
| 2.5 Hurricanes - a model forecast view | 3 |
| 2.6 Key points recall | 3 |
| 3 DATA AND MODEL | 5 |
| 3.1 Data | 5 |
| 3.1.1 IBTrACS | 5 |
| 3.1.2 ERA5 | 5 |
| 3.1.3 GPM-IMERG | 7 |
| 3.1.4 GPM-MERGIR | 8 |
| 3.1.5 GSMAp | 8 |
| 3.2 Numerical model: MONAN | 9 |
| 3.2.1 Initial condition generation | 11 |
| 3.2.2 Post-processing | 11 |
| 4 METHODOLOGY: METRICS AND DIAGNOSTIC FIELDS . | 13 |
| 4.1 Trajectory | 14 |
| 4.2 Intensity | 16 |
| 4.3 Rainfall | 17 |
| 4.4 Hurricane Beryl workflow | 19 |
| 4.5 Hurricane Helene workflow | 19 |
| 5 CASE STUDY: HURRICANE BERYL | 21 |

| | | |
|-------------------|--|-----------|
| 5.1 | Event description - hurricane Beryl | 21 |
| 5.2 | Results and analysis of hurricane Beryl | 22 |
| 5.2.1 | Trajectory | 26 |
| 5.2.2 | Intensity | 27 |
| 5.2.3 | Rainfall | 27 |
| 5.2.3.1 | Pattern and spatial rainfall distribution | 27 |
| 5.2.3.2 | Rainfall mean and overall distribution | 27 |
| 5.2.3.3 | MONAN performance at forecasting rainfall | 27 |
| 5.2.4 | Discussion of key outcomes | 27 |
| 6 | CASE STUDY: HURRICANE HELENE – TESTING THE IMPROVED PARAMETRIZATION | 29 |
| 6.1 | Event description - Helene | 29 |
| 6.2 | Results and analysis of hurricane Helene | 29 |
| 6.2.1 | Trajectory | 29 |
| 6.2.2 | Intensity | 29 |
| 6.2.3 | Rainfall | 29 |
| 6.2.3.1 | Pattern and spatial rainfall distribution | 29 |
| 6.2.3.2 | Rainfall mean and overall distribution | 29 |
| 6.2.3.3 | MONAN performance at forecasting rainfall | 29 |
| 6.3 | Discussion of key outcomes | 29 |
| 7 | CONCLUSIONS AND FUTURE WORK | 31 |
| 7.1 | Future Work | 31 |
| A | APPENDIX - THE MASS FLUX DEDUCTION | 33 |
| B | APPENDIX B - THE TRACKING ALGORITHM | 35 |
| REFERENCES | | 37 |

1 INTRODUCTION

1.1 General objective

To explore a cold pool parameterization coupled with the Grell-Freitas convection parameterization within the Model for Ocean-laNd-Atmosphere predictioN (MONAN).

1.2 Specific objectives

- a) Assess the impact of the cold pool parameterization scheme on hurricane forecasted trajectory, intensity and rainfall;
- b) Perform sensitivity experiments within a hurricane case study, investigating the influence of initial conditions, cold pool duration, the displacement of the maximum mass flux height, type of initial condition and resolution;
- c) Identify the optimal parameter configuration for the cold pool parameterization to be used in MONAN;
- d) Evaluate the performance of this optimal configuration in other hurricane case study.

1.3 Scientific questions

This work builds upon the findings and open issues identified in Freitas et al. (2024). The following scientific questions are proposed:

- Does the GF-Cold Pool (GF-CP) scheme improve the forecast of hurricane trajectory, intensity, and rainfall in MONAN?
- Which parameters within the GF-CP have the most significant influence on hurricane representation in MONAN?
- How robust is the optimal GF-CP configuration when applied to a different hurricane event?
- Can improvements in cold pool representation lead to better rainfall predictions in tropical cyclones?

1.4 Thesis organization

2 LITERATURE REVIEW

2.1 Overview of convective cloud dynamics

2.2 Cold pools

2.3 The mass-flux approach

2.4 The cold pool parameterization

2.5 Hurricanes - a model forecast view

2.6 Key points recall

3 DATA AND MODEL

3.1 Data

This section presents the observational datasets used as a reference for evaluating the model forecasts. The selected datasets, described in detail in Sections 3.1.1 to 3.1.5, are commonly employed in tropical cyclone studies and provide reliable information on storm trajectory, intensity, and precipitation. They have been used in several studies (ZHOU; MATYAS, 2021; BOPAPE et al., 2021; DULAC et al., 2024; YANG et al., 2024; MAY et al., 2024) and support a robust assessment of the model's performance

3.1.1 IBTrACS

The International Best Track Archive for Climate Stewardship (IBTrACS) (KNAPP et al., 2010) offers comprehensive data on the location and intensity of global tropical cyclones. It emphasizes parameters such as geographic position (latitude and longitude), maximum sustained wind speed (measured in knots), and minimum central pressure (in millibars). A complete list of variables and their definitions can be found at the provided link

This dataset features a spatial resolution of 0.1° (approximately 10 km) and primarily reports data at a temporal resolution of 6 hours, although it can be interpolated to intervals of 3 hours; for our purposes, we will be utilizing the 6-hour data. The dataset covers the period from 1841 to the present, allowing users to explore it by searching for specific oceanic basins, including the North Atlantic, South Atlantic, Eastern North Pacific, Western North Pacific, South Pacific, South Indian, and North Indian.

The dataset is built upon information from various agencies. According to the documentation, the sources of this information include all available resources utilized by forecasters, such as surface observations, aircraft reconnaissance flights, and satellite observations.

3.1.2 ERA5

ERA5 (HERSBACH et al., 2020) represents the fifth generation of atmospheric reanalysis conducted by the European Centre for Medium-Range Weather Forecasts (ECMWF), serving as a vital resource for both global climate and weather studies. This reanalysis integrates a forecast model with an advanced data assimilation

scheme. Specifically, ERA5 employs the ECMWF Integrated Forecast System (IFS) CY41R2 forecast model, executing twice-daily short-term forecasts (18 hours) derived from analyses conducted at 06:00 and 18 UTC. Check the link for a comprehensive understanding of the physical parameters encompassed within the model. The 4D-Var data assimilation method assimilates a diverse array of observations, including satellite data, ground station measurements, instrumented buoy data, and reconnaissance aircraft information. This process utilizes 12-hour time windows from 09 UTC to 21 UTC and from 21 UTC to 09 UTC (the subsequent day).

The initial configuration of the product involves 137 hybrid sigma/pressure levels in the vertical, with the uppermost level being at 0.01 hPa, and it maintains a horizontal resolution of 0.28125° (approximately 30km). Atmospheric data are accessible across interpolated 37 pressure levels. Consequently, the dataset comprises four primary subsets for download: hourly and monthly products, available on pressure levels (restricted to 37 levels) and single levels that encompass atmospheric, ocean-wave, and land surface quantities.

Reanalyses are not constrained by the necessity for timely forecasts, which allows for an extended period to collect observations. Furthermore, when assessing historical data, enhanced versions of the original observations can be integrated, thereby enhancing the quality of the reanalysis product. As a result, reanalyses provide a physically and dynamically consistent global representation of the atmospheric state at each time step. The major advantage of atmospheric reanalysis, particularly in the context of studying tropical cyclones, lies in its capacity to facilitate the analysis of the internal three-dimensional structure of contemporary TCs, alongside the large-scale environmental conditions surrounding them ([DULAC et al., 2024](#)).

The ERA5 data is accessible via the Climate Data Store and downloadable through the Climate Data Store (CDS) Application Program Interface (API). The variables under investigation are highlighted in the table below.

Table 3.1 - List of ERA5 Variables Used

| Variable name | Long name | Unit |
|---------------|----------------------------------|-------------------|
| msl * | Mean sea level pressure | Pa |
| i10fg * | Instantaneous 10 metre wind gust | m s ⁻¹ |
| tp * | Total precipitation | m |

Table continued on next page

| Variable name | Long name | Unit |
|---------------|---------------------------------------|-------------------|
| sst * | Sea Surface Temperature | K |
| press ** | Pressure | Pa |
| u ** | U component of wind (Zonal Wind) | m s ⁻¹ |
| v ** | V component of wind (Meridional Wind) | m s ⁻¹ |

*Legend: * single levels; ** pressure levels.*

Source: Made by the author (2025).

3.1.3 GPM-IMERG

NASA's Integrated Multi-satellite Retrievals for GPM (Global Precipitation Measurement) (IMERG) ([HUFFMAN, 2019](#)) algorithm synthesizes information from the GPM satellite constellation. Satellite data are particularly valuable to get information in areas of the Earth where ground-based precipitation-measuring instruments are limited, such as the Atlantic's Main Development Region.

According to the Technical Documentation , estimates from various precipitation-relevant passive microwave (PMW) sensors within the GPM constellation are processed using an algorithm. These estimates are then gridded, intercalibrated with the GPM Combined Radar Radiometer Analysis product, and integrated into half-hourly fields with a horizontal resolution of $0.1^\circ \times 0.1^\circ$, covering latitudes from 60°S to 60°N . This data is provided to the Climate Prediction Center (CPC) Morphing-Kalman Filter (CMORPH-KF) quasi-Lagrangian time interpolation procedure, as well as undergoing a re-calibration that applies to the Precipitation Estimation from Remotely Sensed Information using Artificial Neural Networks (PERSIANN) Dynamic Infrared–Rain Rate (PDIR) infrared precipitation retrievals.

The product is offered in three stages: Early Run, Late Run, and Final Run. Researchers are encouraged to utilize the Final Run data for comprehensive analyses, as this stage incorporates monthly gauge data to create research-level products. However, it is important to note that the Final Run data has a latency period of approximately 3.5 months from the time of observation. Accordingly, we will employ the Final Run product, specifically using the NASA Goddard Earth Sciences (GES) Data and Information Services Center (DISC) V07 data, accessible through the link [,](#) last accessed on 16 May 2025, which offers precipitation data in netCDF format.

Lastly, concerning temporal distribution, this dataset, which covers the period from June 2000 to September 2021, is available for download every half-hour, daily, or monthly. For

our analysis, we intend to concatenate the data to create hourly aggregates from the half-hourly product, which will subsequently be extrapolated to a resolution of approximately 30 km (our forecast resolution).

3.1.4 GPM-MERGIR

In the context of convective cloud modeling, it is essential to evaluate the model's capability to accurately represent cloud morphology. This assessment can be achieved through the analysis of infrared (IR) brightness temperature (Tb), also known as equivalent black-body temperature, using satellite data. The observational dataset we are currently employing comes from the NASA GES DISC GPM Merged 4-Km IR Tb data set (GPM-MERGIR) ([JANOWIAK et al., 2017](#)), which is sourced from the NOAA Climate Prediction Center (CPC)/NCEP/NWS. The satellites contributing to this dataset include the Geosynchronous Operational Environmental Satellites (GOES) from the United States, the Geosynchronous Meteorological Satellite (GMS), followed by the Multi-functional Transport Satellite (MTSat) and Himawari from Japan, as well as the Meteorological Satellite (Meteosat) from the European Community, which forwards infrared (IR) imagery to the CPC. A complete list of these satellites can be found at this link

The data is made available periodically in half-hour increments, covering latitudes from 60°S to 60°N with a pixel resolution of 4 km, dating back to 1 January 1998. In addition to direct downloads of netCDF-4 format data, GES DISC also provides data in binary, ASCII, and netCDF-3 formats via the OPeNDAP interface.

3.1.5 GSMAp

Another satellite-based combined microwave-IR precipitation dataset will be utilized to evaluate precipitation generated by tropical cyclones. The Global Satellite Mapping of Precipitation (GSMAp), supported by the JAXA Precipitation Measuring Mission (PMM) Science Team, offers a multi-satellite global precipitation map as part of the Global Precipitation Measurement (GPM) Mission. It employs the Dual-frequency Precipitation Radar (DPR) onboard GPM core satellites, along with other GPM constellation satellites and geostationary satellites (website). Additionally, in the GSMAp products, apart from GSMAp_NOW, the Globally-merged, full-resolution ($\sim 4\text{km}$) infrared data produced by NOAA/CPC has also been utilized. The original data used for this product have been supplied by JAXA's GSMAp.

The key feature of the GSMAp algorithm is its use of various attributes derived from the spaceborne precipitation radar, including TRMM/PR and GPM/DPR. This algorithm generates a rainfall rate product (in mm/hr) that covers a global extent (60°N to 60°S) with a horizontal resolution of 0.1° (latitude/longitude) and is available on an hourly basis.

The differences, features, and performance of this dataset compared to GPM-IMERG in tropical cyclone cases are widely discussed in the literature (REDDY et al., 2022; BAGTASA, 2022; YANG et al., 2024).

3.2 Numerical model: MONAN

The model utilized for this study is part of the next generation of numerical models currently under development. The Model for Ocean-LaNd-Atmosphere Prediction (MONAN) is an advanced project by the Brazilian Centre of Weather and Climate Prediction (CPTEC) to become the new standard for weather and climate forecasting, nowcasting, and hindcasting. MONAN is an adaptation of the Model for Prediction Across Scales (MPAS), and further details will be provided in the subsequent paragraphs.

The MONAN is a collaborative initiative led by the National Institute for Space Research (INPE) and the Ministry of Science, Technology, and Innovation (MCTI). Its primary objective is to improve weather and climate forecasting in Brazil, South America, and the Caribbean at all spatial and temporal scales, particularly in climate change scenarios.

MONAN employs an MPAS (Model for Prediction Across Scales) dynamical core, supplemented by various physics innovations developed by the scientific community. The most recent version of MONAN is 1.0.0 (last seen on July 2, 2024) with ongoing enhancements available for review at <https://monanadmin.github.io/>.

Regarding the physics suite, MPAS offers two configurations: “Mesoscale Reference” and “Convection-permitting,” which vary based on resolution. The Mesoscale Reference is suitable for mesoscale resolutions (greater than 10 km cell spacing; i.e., $dx > 10$ km) but, as noted in the MPAS manual is not ideal for convective-scale simulations since the Tiedtke scheme can eliminate convective instability before the resolved-scale motions (convective cells) can effectively respond. On the other hand, the Convection-permitting option is designed for spatial resolutions that accommodate both explicitly resolved hydrostatic and nonhydrostatic motions. This suite is recommended for any MPAS applications employing convection-permitting meshes ($dx < 10$ km), including variable-resolution meshes that span hydrostatic to nonhydrostatic resolutions.

For our simulations ($15\text{km} < dx < 60\text{km}$), the current physics parameters are summarized in the table below:

The cloud microphysics utilizes the single-moment 6-class scheme as described by ??). The convection parameterization, based on the mass-flux approach developed by Grell (2014) and Freitas (2018), is implemented here along with the cold pool scheme proposed by Freitas (2024). Both the Planetary Boundary Layer (PBL) and Surface Layer parameterizations employ the Mellor-Yamada-Nakanishi-Niino level 2.5 closure turbulent kinetic

Table 3.3 - Physics bulk configuration

| Parameter | Configuration |
|--------------------------------|----------------------|
| Mesoscale reference (30 km) | |
| Microphysics | WSM-6 |
| Convection | Grell-Freitas MONAN |
| Boundary layer (BL) | MYNN |
| Gravity wave drag by orography | YSU |
| Longwave radiation (LW) | RRTMG |
| Shortwave radiation (SW) | RRTMG |
| Cloud fraction for radiation | Cloud Fraction Monan |
| Surface layer | MYNN |
| Land surface | Noah |

Source: Made by the author (2025).

energy (TKE) based scheme. Orographic gravity-wave drag is represented using the Yonsei University (YSU) PBL scheme. For solar (shortwave) and terrestrial (longwave) radiative transfers, the Rapid Radiative Transfer Model for GCMs (RRTMG; Iacono et al., 2008) radiation scheme is utilized. Finally, the Land Surface parameterization is based on the Noah community model.

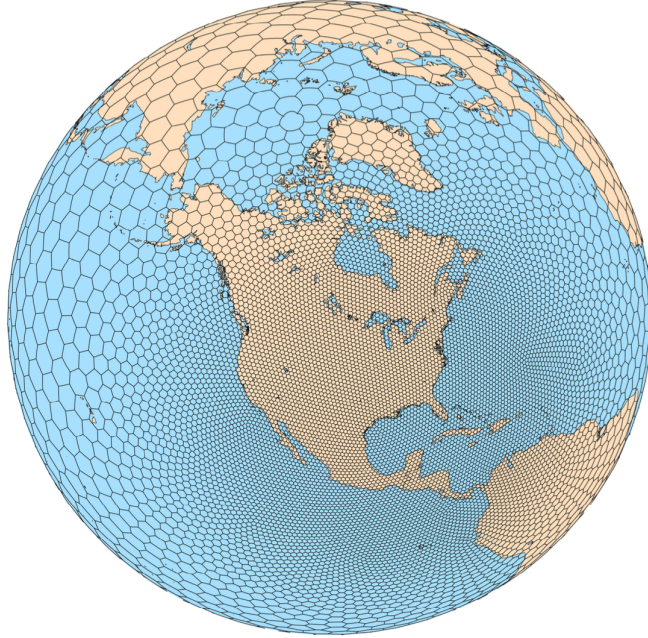
All simulations were conducted globally, utilizing a uniform horizontal grid spacing dependent on the specific experiment, which was set at 15 km, 30 km, and 60 km. The model has 55 vertical levels, with the ocean reference set at depths of 0 m and 30000 m (30 km). Due to the global scope, only a single initial condition was required, sourced from the ERA5 and GFS models. The duration of the model time integration varies according to the experiment and will be detailed in the results section, along with the initial time of integration. Figure XXX displays a map generated with MPAS-A and Figure 3.1 a map of convective rain accumulated of 2 days forecasted by MONAN.

As one can see, one of the big differences between MPAS and its predecessor, the WRF model, is that the model is discretized on centroidal Voronoi meshes using a C-grid staggering of the prognostic variables, allowing variable horizontal resolution, and also solving the equations of motion directly on these unstructured meshes (Skamarock, 2012).

For our study, a set of variables was chosen to perform it. Table XXX indicates the variable name inside MONAN, alongside with the long name and the unit.

Total rainfall was computed by simply summing the variables rainnc and rainc for each lat/lon point. The wspd is the module of the squared sum of zonal and meridional winds at the first model level. From uzonal_200hPa below, all variables are computed at the

Figure 3.1 - MPAS-A meshes and the ability to configure the meshes at different resolutions



Source: <<https://www2.mmm.ucar.edu/projects/mpas/site/visualization.html>> (2025) .

reference level pressure; for instance, `uzona_200hPa` means the zonal wind at the pressure level of 200hPa.

3.2.1 Initial condition generation

To begin the integration process, Initial Conditions (IC) must be prepared by MPAS requirements (one could use the MPAS user guide for more details). We generated the initial conditions using the Weather Research & Forecasting Model (WRF) Pre-Processing System (WPS), utilizing data obtained from ERA5, which we pre-processed with the WPS. These initial conditions were then uploaded into the MONAN IC folder and executed accordingly. For the IC sensitivity test, we also acquired a GRIB file from the Global Forecast System (GFS) model, a courtesy provided by Saulo R. Freitas, who already had the data available. The model will initially be set up with a global 30 km MPAS grid, with plans to modify this in future sections. It is important to note that a new IC will need to be created for each resolution.

3.2.2 Post-processing

Since the model output is generated on a non-structured grid, a post-processing step is necessary to map the native MPAS output to other meshes, enabling visualization on a

standard lat/lon map. To achieve this, MONAN employs the convert-MPAS project. This approach utilizes a nearest-neighbor scheme to remap integer fields to the target grid, with additional information available at this link.

In this study, the Climate Data Operators (CDO) were also utilized to remap various datasets, including ERA5, GPM-IMERG, GPM-MERGIR, and GSMP, as well as several forecasts (such as those simulated at 15km and 60km horizontal resolutions) to the MONAN forecasts.

4 METHODOLOGY: METRICS AND DIAGNOSTIC FIELDS

The analysis will focus on three main characteristics of cyclones commonly utilized (DESH-PANDE et al., 2010; BOPAPE et al., 2021; ZARZYCKI et al., 2021; NYONGESA et al., 2024; MISHRA et al., 2024) in weather forecasting: track, intensity, and rainfall. The table below outlines the questions designed to guide the examination of each characteristic in alignment with the dissertation's objectives. This approach will help refine the metrics and outputs available in the existing literature.

Table 4.1 - Key Research Questions for Track, Intensity, and Rainfall Assessment

| Topic | Question | ID |
|------------|--|-----|
| Trajectory | What is the overall performance of the parameterization and sensitivity tests in reproducing the hurricane's track? | T.1 |
| | What is the error (in kilometers) associated with these tracks? | T.2 |
| | Which configuration shows the best performance? | T.3 |
| | After how many forecast hours do larger deviations begin to appear? | T.4 |
| | Is there any observable trend in the tracks? | T.5 |
| | How does the large-scale environment influence these deviations? | T.6 |
| | What is the overall performance of MONAN? | T.7 |
| Intensity | What is the overall performance of the parameterization and sensitivity tests in reproducing the hurricane's intensity? | I.1 |
| | How much bias is present in these results? | I.2 |
| | How well does ERA5 perform in reproducing this intensity, and why? | I.3 |
| | Is there any thermodynamic or mechanical explanation for these trends? | I.4 |
| | What is the overall performance of MONAN? | I.5 |
| Rainfall | What is the overall performance of the parameterization and sensitivity tests in reproducing the hurricane's rainfall pattern? | R.1 |
| | In which regions is there a negative (or positive) bias in the rainfall field? | R.2 |
| | What is the overall performance of the parameterization and sensitivity tests in reproducing the hurricane's cloud morphology? | R.3 |

Table continued on next page

| Topic | Question | ID |
|-------|---|-----|
| | How much light, moderate, and heavy rainfall is being produced by the simulations? | R.4 |
| | What is the average rainfall produced by the simulations? | R.5 |
| | What is the bias between the extreme rainfall produced by the simulations and the reference data? | R.6 |
| | What is the overall performance of MONAN? | R.7 |

Source: Made by the author (2025).

In the following subsections, the approaches and metrics used to evaluate each of these characteristics will be explained in detail. Finally, a workflow diagram will be presented, summarizing the described methods and indicating at which stage each question will be addressed. All code made for this dissertation is available on the git repository: [GitHub - Dissertation Repository](#) mainly written in Python

4.1 Trajectory

A map illustrating the forecasted trajectories will be generated using a tracking algorithm developed by the author. A discussion regarding the performance of this tracking and guidance can be found in Appendix A. Additionally, a time series analysis will be conducted to evaluate the errors associated with each trajectory. These errors are defined as the distance between the central pressure reference points and the forecasted central pressure points, calculated using the GeoPy library¹. As noted in the literature, the calculations could be performed following the methodology proposed by Moon et al. (2021) but here we simply calculate the great-circle distance between two points.

To quantitatively validate the results, a graphical representation will display the Mean Absolute Error (MAE) and Root Mean Square Error (RMSE) for each of the trajectories, regarding the reference dataset.

The MAE is widely employed (DITCHEK et al., 2023; NYONGESA et al., 2024) in the literature and can be defined as:

$$\text{MAE} = \frac{1}{N} \sum_{i=1}^N |F_i - O_i| \quad (4.1)$$

in this equation, N represents the sample size (number of points in the trajectory), F denotes the forecast outputs generated by the model, and O refers to the observation outputs obtained from a reference dataset. The error values can range from 0 to ∞ , with a

¹<https://geopy.readthedocs.io/en/stable/>

perfect score indicated by 0. The aim is to calculate the average magnitude of the forecast errors. It is important to note that this error does not convey the direction of the deviations due to its absolute nature; this aspect will be examined using another method discussed later.

Along with the MAE, usually, RMSE is computed to seek a kind of average error, but now weighted according to the square of the error. As the same as before, it varies from 0 to ∞ , and a perfect score means RMSE equal to 0. It is defined as:

$$\text{RMSE} = \sqrt{\frac{1}{N} \sum_{i=1}^N (F_i - O_i)^2} \quad (4.2)$$

The letters in this equation have the same meaning as in the previous equation. To better understand the potential trends in the trajectory, in addition to visual comparisons, one can utilize cross-track and along-track errors computed into a time series. The errors assess the deviation of the forecasted position from the observed path (cross-track) and the speed of the forecast from the observations (along-track). The cross-track error is measured perpendicularly to the observed trajectory, while the along-track error is measured along the actual course at a specified event. Together, these metrics² can also indicate the directional error of each forecast. Figure 4.1 more clearly illustrates the distinction between cross-track and along-track errors.

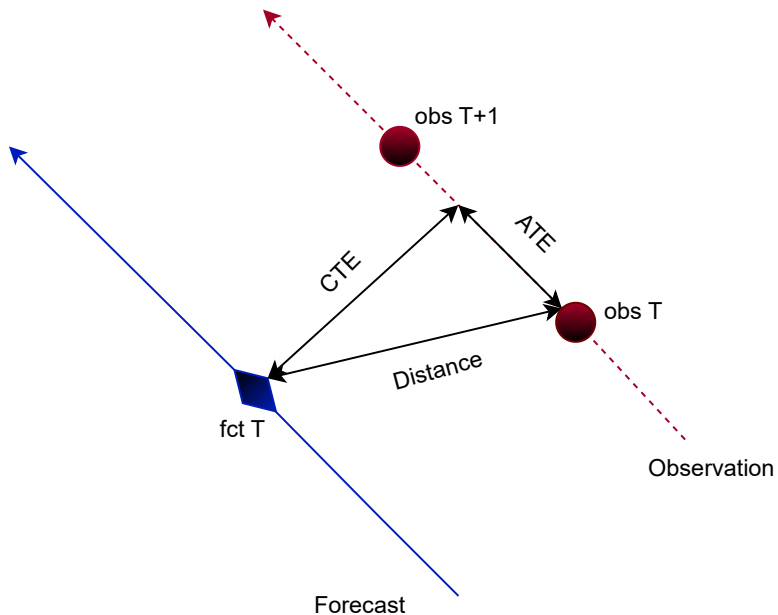
In the context of our expected findings, negative (positive) values of cross-track errors indicate that the forecasted center of the hurricane is projected to be located to the west (east), while negative (positive) values of along-track errors suggest that the center is slower (faster) than its intended trajectory.

Those errors can be clarified by examining the meteorological fields. Following the approach of Gao et al. (2023), analyzing the 700 hPa geopotential height can reveal the large-scale features contributing to the bias in the trackings. For instance, in the authors' study, forecasts displaying significant eastward track bias for tropical cyclones often correspond with a noticeably weaker subtropical high over the North Atlantic. These fields can be computed easily using Python.

In conclusion, utilizing a straightforward statistical mean of the errors (specifically the MAE and RMSE) can provide valuable insights into the overall performance of the MO-NAN simulations. The mean is defined as follows:

²The equations used to compute those errors can be found at this website: <<https://www.movable-type.co.uk/scripts/latlong.html>>

Figure 4.1 - Illustration of cross-track and along-track errors. The definitions of Cross-Track Error (CTE) and Along-Track Error (ATE) are based on the distance between an observation (obs) and a forecast (fct) at the same valid time (T). This distance is computed as the great-circle distance.



Source: Made by the author (2025).

$$\text{MEAN} = \frac{1}{E} \sum_{i=1}^E \text{errors}_i \quad (4.3)$$

where E denotes the total number of experiments conducted using the MONAN framework. This approach facilitates a comprehensive understanding of the general behavior exhibited by the MONAN runs and can be compared with ERA5, for instance.

4.2 Intensity

In reviewing the literature, tropical cyclone intensity is defined as the maximum surface wind speed associated with the central pressure (DEMARIA et al., 2007; LANDSEA; FRANKLIN, 2013). However, some studies argue that depending exclusively on wind speed does not fully capture the concept of intensity, suggesting that pressure can also serve as a significant indicator of forecasted intensity (SHEPHERD; WALSH, 2017; HEMING, 2017). This dissertation will adopt the latter approach by evaluating both pressure and wind as intensity indicators.

To conduct these evaluations, we will analyze time series data that includes the central pressure identified by the tracking system and the maximum wind speed, which is derived from the first level of the model. A discussion on how to determine this maximum wind speed in the model can be found in Appendix A. The time series will serve as a measure of forecast performance, allowing us to assess how closely the computed values align with actual observations and where they occur.

In addition to a visual comparison, we will create a graph containing the MAE and RMSE to quantify the forecasts and rank them based on their effectiveness in illustrating intensity. Additionally, the mean of those errors can also be computed and compared with ERA5 to give us insights into the general MONAN performance.

To validate these results, we can examine meteorological fields such as the geopotential height between 850 hPa and 500 hPa, as well as the pressure and wind fields at 850 hPa, to gain insights into the forecast's impact on cyclone movement and intensity; all of the fields can easily be computed using Python.

4.3 Rainfall

The analysis of rainfall for our runs is based on the methodology proposed by Marchok et al. (2007). According to these authors, evaluating forecasted rainfall requires examining three key aspects: the rainfall pattern, the mean and distribution of rain volume, and the extreme values.

To investigate the rainfall pattern, we will utilize the Equitable Threat Score (ETS; Mesinger (2008)) along with pattern correlation analysis (namely the Pearson Correlation Coefficient) and visual comparisons using selected snapshots, considering also the related bias of those fields. The mean and distribution of rain volume can be assessed through the computation of the Cumulative Density Function (CDF) and the Probability Density Function (PDF). Extreme rainfall values will be specifically analyzed by examining the 85th percentile computed at the CDF. Lastly, we will discuss a performance score for MONAN in comparison to ERA5 by averaging the results of all experiments. Table 4.3 summarizes the metrics to be computed, followed by a brief explanation of each metric and its intended purpose.

Table 4.3 - Metrics used to evaluate rainfall forecast performance

| Metric | Definition |
|--|--|
| ETS (Equitable Threat Score) | Measures the skill of categorical forecasts by comparing the number of hits to what would be expected by chance: $\text{ETS} = \frac{H - H_r}{H + F + M - H_r}$ where H is the number of hits, F is false alarms, M is misses, and $H_r = \frac{(H+F)(H+M)}{\text{total}}$ is the expected number of hits due to chance. |
| Pearson Correlation Coefficient | Measures the spatial similarity between observed and forecasted rainfall fields: $r = \frac{\sum_{i=1}^n (F_i - \bar{F})(O_i - \bar{O})}{\sqrt{\sum_{i=1}^n (F_i - \bar{F})^2 \sum_{i=1}^n (O_i - \bar{O})^2}}$ where F and O are forecasted and observed values, calculated over n data points, where i is the index running from 1 to n . |
| Bias | Quantifies the difference between forecast and observation: $\text{Bias} = F - O$ |
| CDF (Cumulative Distribution Function) | Represents the probability that a variable takes a value less than or equal to a given threshold: $\text{CDF}(x) = P(X \leq x)$ |
| PDF (Probability Density Function) | Describes the relative likelihood for a variable to take a specific value: $\text{PDF}(x) = \frac{d}{dx} \text{CDF}(x)$ |

Source: Made by the author (2025).

The ETS evaluates how well forecasted “yes” events correspond to observed “yes” events, while accounting for agreements due to random chance. According to [Marchok et al. \(2007\)](#), this implies that the ETS penalizes a model for overproducing rainfall above a given threshold, even if the rainfall pattern is realistic. For this metric, a hit is defined as an event that was forecasted to occur and did occur; a miss is an event that was not forecasted but occurred; and a false alarm is an event that was forecasted but did not occur.

Pattern correlation is computed as the Pearson correlation coefficient (r) between the forecasted and observed rainfall fields. The correlation ranges from -1 to 1, where: (i) $r = 1$ indicates a perfect positive linear relationship; (ii) $r = -1$, a perfect negative linear relationship; and (iii) $r = 0$ implies no linear relationship between forecast and observation.

The bias is the difference between the forecast (F) and the observations (O), typically averaged over time or space. A negative bias indicates underestimation, while a positive bias indicates overestimation. The bias can range from negative to positive infinity, with 0 representing a perfect forecast.

Both the CDF and the PDF will be used to analyze rainfall distributions. The CDF shows the cumulative probability of rainfall values up to a certain threshold. For example, the corresponding x-axis value when the y-axis equals to 0.5 (or 50%) on the CDF corresponds to the median rainfall amount. The CDF ranges from 0 to 1 on the y-axis, indicating the proportion of the data below a given threshold on the x-axis. For instance, the 0.85 mark on the CDF corresponds to the 85th percentile, meaning 85% of the data falls below that threshold, and the remaining 15% above it. This is a straightforward way to seek for rainfall extremes.

The PDF, similar to a histogram, describes the probability of observing values within a specific range. It is normalized such that the total area under the curve equals 1. To interpret the PDF, one can compute the area under the curve within a specified range, which represents the probability of a value falling in that interval. Mathematically, the CDF is the integral of the PDF. One should notice that both CDF and PDF can be computed empirically or theoretically. The difference between them is that when computing empirically, one will consider the natural distribution of data, and theoretically, one will consider a mathematical distribution (gamma, Gaussian, etc). In this study, we will utilize the empirical approach.

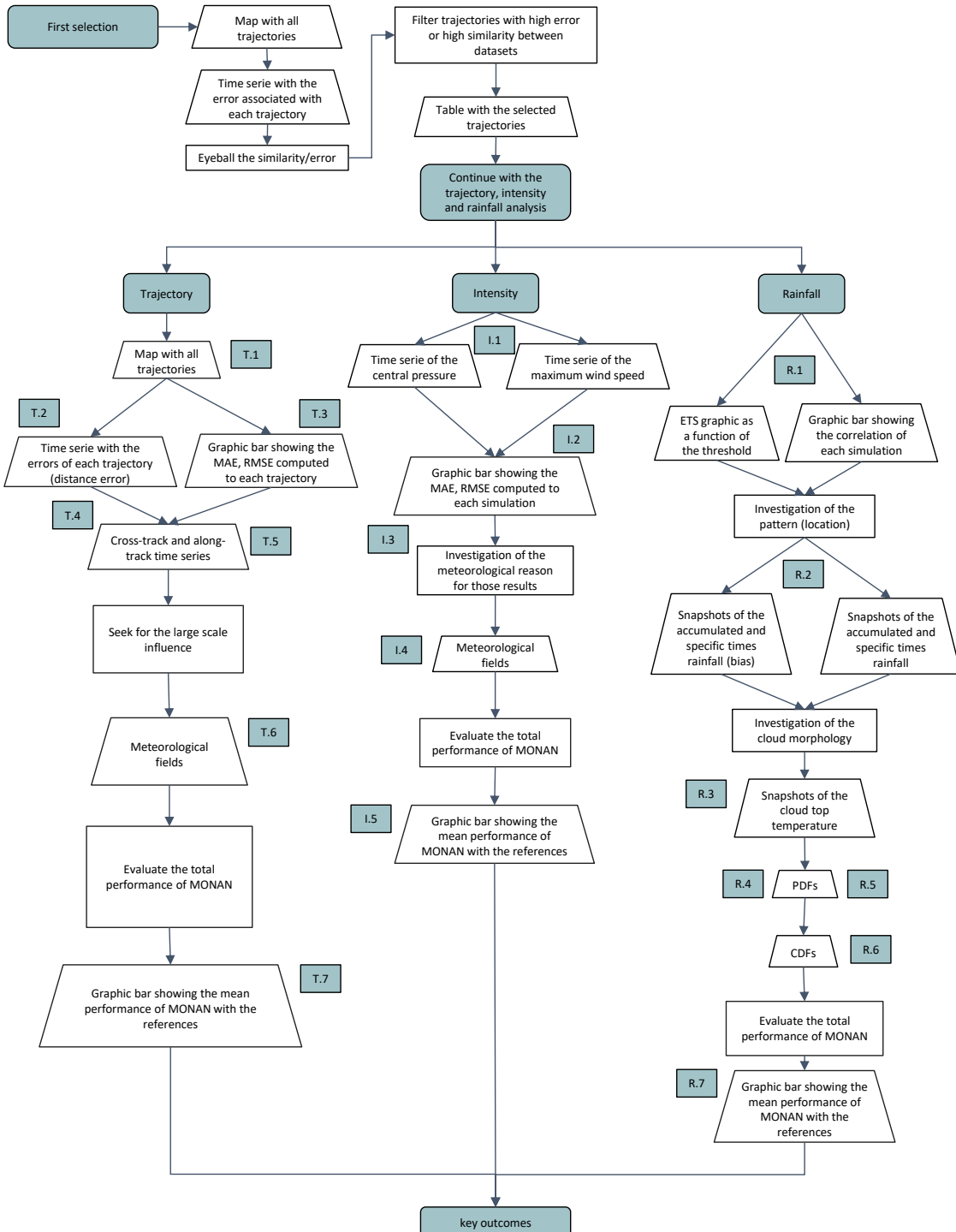
4.4 Hurricane Beryl workflow

The workflow below summarizes and organizes the upcoming steps. After a quick initial analysis, the results will be visually represented as trapezoidal shapes, while discussions will be depicted with rectangular shapes. This distinction helps clarify the types of information being presented at each stage of the process. Following this, the boxes containing question IDs, as outlined in Table 4.1, related to the three aspects under evaluation (trajectory, intensity, and rainfall) will be also displayed in the workflow.

The reader should note that an initial selection of the results will be conducted. As the diagram indicates, a trajectory map will be created, accompanied by distance errors. The selection criteria will focus on experiments that do not contribute significantly to the discussion, either because they are part of a set of similar experiments or due to excessively large errors that do not accurately represent the model state we aim to address.

4.5 Hurricane Helene workflow

Figure 4.2 - Workflow Overview



Source: Made by the author (2025).

5 CASE STUDY: HURRICANE BERYL

This chapter explores the results of implementing cold pool parameterization in the latest Brazilian numerical weather and climate prediction model. It focuses on its performance in forecasting hurricane trajectory, intensity, and rainfall. It specifically focuses on the case study of Hurricane Beryl, which occurred in June and July 2024 in the North Atlantic Ocean. Following a brief event description as an introduction, the chapter describes the data utilized, the numerical model employed, and the evaluation framework established. Finally, the findings are presented and discussed.

5.1 Event description - hurricane Beryl

5.2 Results and analysis of hurricane Beryl

In this section, we will present the results in alignment with the established workflow and engage in a discussion regarding the questions outlined in Table 4.1. The subsequent subsections will detail the trajectory, intensity, and rainfall analyses. To conclude, we will provide a summary discussion highlighting the key outcomes of the model and evaluating the overall performance of MONAN in comparison with ERA5.

By the workflow sequence, we will begin by addressing the selection process. Table 5.1 illustrates all the experiments that were conducted.

Table 5.1 - All Performed Experiments

| Experiment | Description | ID |
|---------------------------|---|---|
| Cold Pool Effect | Turn on and off the cold pool parameterization scheme | CP-ON CP-OFF (Control) |
| Initial Condition Day | Compares the effect of four initial conditions, June 29, 1st July, July 2nd (noon) and July 3rd. | CP-29 CP-01 CP-02T12 CP-03 (Control) |
| Cold Pool Lifetime | Compares the effect of cold pool lifetime being 1h, 2h (default), 3h, and 6h | CP-1H CP-2H (Control) CP-3H CP-6H |
| Maximum Down-draft Height | Compares the effect of the maximum downdraft height, being 0.25, 0.35, and 0.50 | CP-D025 CP-D035 (Control) CP-D050 |
| Resolution Experiment | Evaluates the resolution effect on the results, degrading it into 60 km and enhancing it into 15 km | CP-15km CP-30km (Control) CP-60km |
| Type of Initial Condition | Changes the type of initial condition to be from the GFS model | CP-ERA5 (Control) CP-GFS |
| Best Configuration Test | A run with two changes inside the cold pool parameters | CP-1HD050 CP-1HD05015km |

Source: Made by the author (2025).

The “ID” column serves as a reference for the names of the experiments. It is important to note that in the results, CP-ON represents the default configuration. In the sensitivity

analyses conducted, the default values are specified in the labels. For instance, in the “Resolution Experiment”, the default configuration is set to a grid of 30 km (CP-30km), which is then changed to 60 km (CP-60km) and 15 km (CP-15km). To clarify, the following table emphasizes the default parameters:

Table 5.3 - Default values for the cold pool parameterization scheme

| Parameter | Default Value |
|---------------------------|-------------------------|
| Initial Condition Day | July 3rd (00 UTC), 2024 |
| Cold Pool Lifetime | 2 h |
| Maximum Downdraft Height | 0.35 |
| Resolution Experiment | 30 km grid |
| Type of Initial Condition | Coming from ERA5 |

Source: Made by the author, 2025.

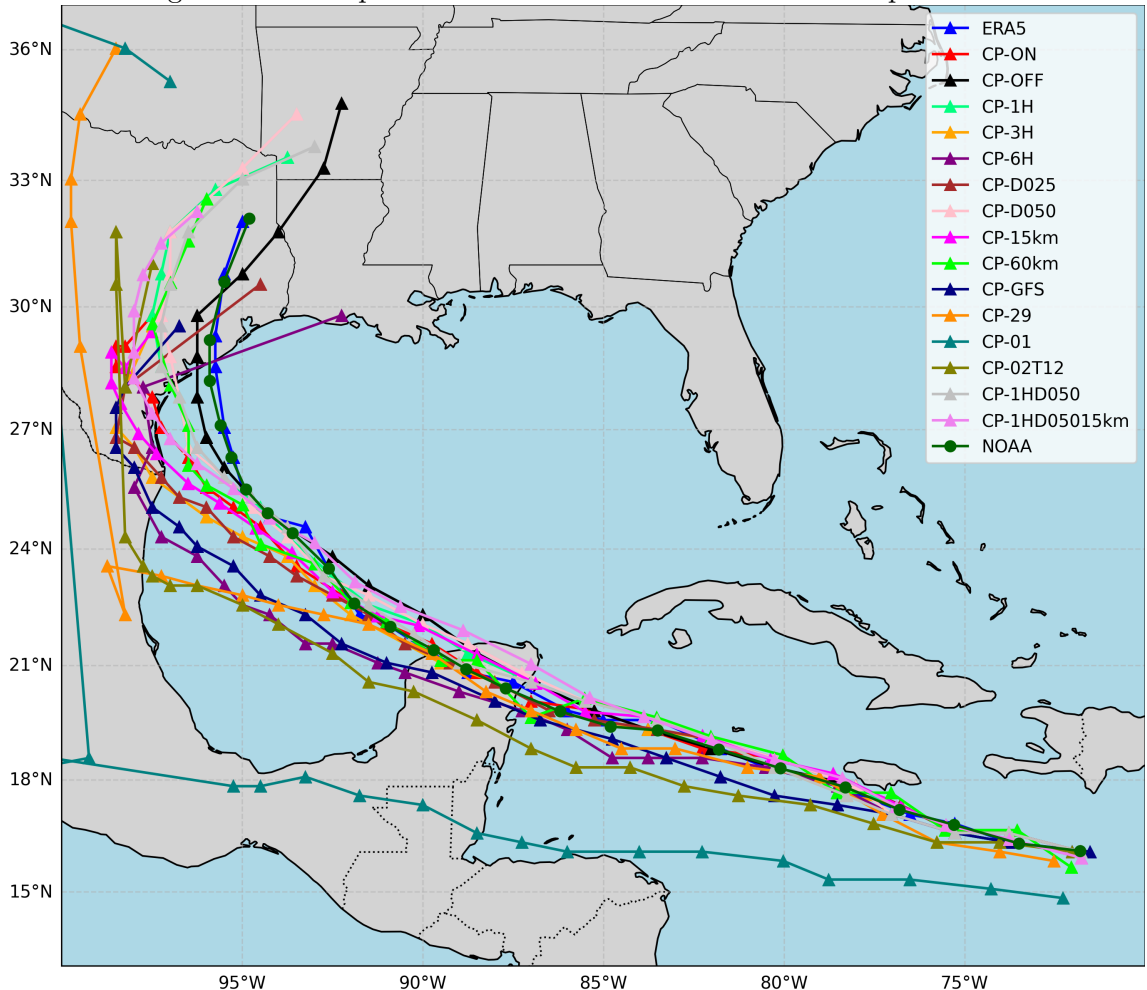
We investigate the impact of cold pools by enabling (CP-ON) and disabling (CP-OFF) the parameterization, with CP-OFF serving as the control experiment in this case. In the subsequent rows, we conducted a sensitivity analysis on the parameters within the parameterization. Now our control experiment is the CP-ON configuration, with the Table 5.3 parameters. For the “Initial Condition Day” experiment, we varied the initial integration times: June 29 (00 UTC), 2024; July 1 (00 UTC), 2024; and July 2 (12 UTC), 2024 - comparing them with the default time. These periods were selected because they correspond to key moments in the storm’s evolution: shortly after HB was classified as a tropical storm, one day before it reached Category 5, and the day it reached Category 5, respectively.

The “Cold Pool Lifetime” was adjusted from the default to durations of 1 hour, 3 hours, and 6 hours. The height of the mass flux above the surface is described by a parabolic function, and the coefficient of this function can be manipulated to alter the maximum height, with lower (higher) values indicating proximity (distance) to the surface. The “Type of Initial Condition” was switched from ERA5 to GFS, both initialized on July 3 (00 UTC), 2024.

During the computation of the initial 13 experiments, we observed that setting the cold pool lifetime to 1 hour and adjusting the maximum downdraft height coefficient to 0.5 resulted in lower errors in the initial results. Consequently, we conducted the “Best Configuration Test” with these parameter adjustments and repeated this configuration at 15 km, bringing the total number of experiments to 15. The reference data here is the best track dataset, and hereafter this dataset will be referenced as “NOAA”.

Keeping this in mind, Figure 5.1 shows all the trajectories for the 15 experiments, plus ERA5 and the reference best-track dataset.

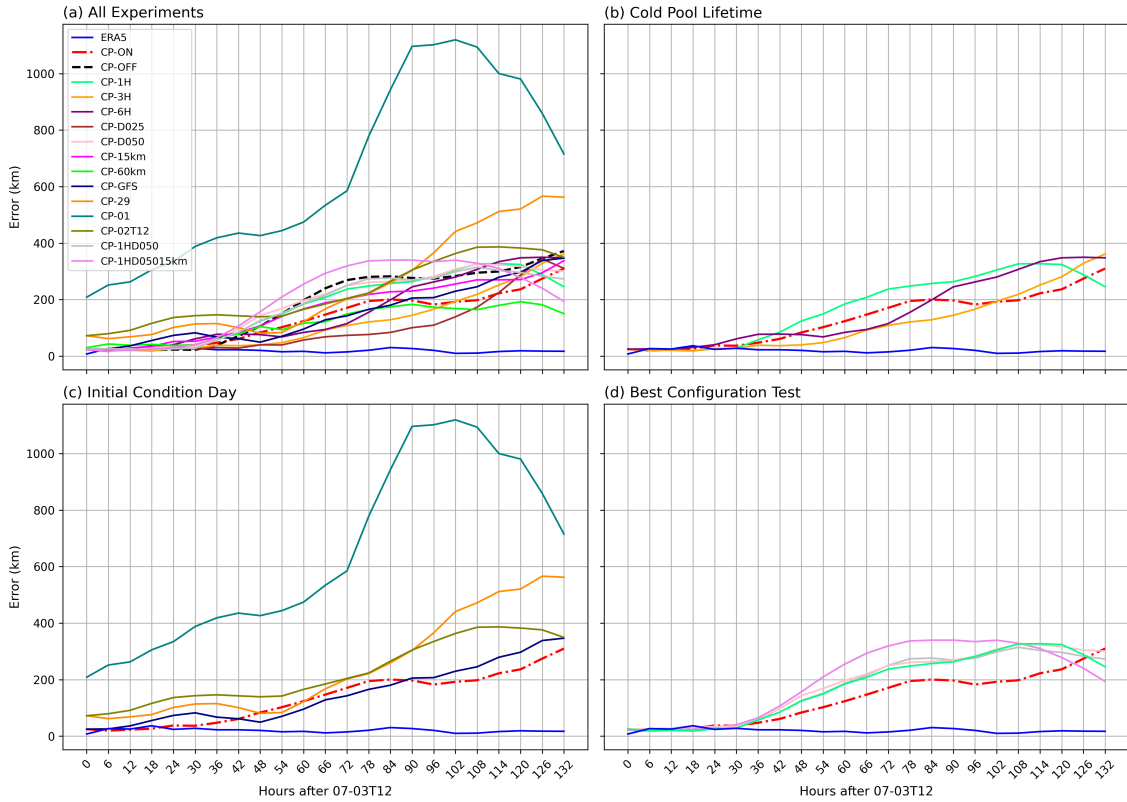
Figure 5.1 - Comparison of Storm Tracks Across All 15 Experiments



Source: Made by the author (2025).

As one can see in Figure 5.1, the numerous experiments clutter the scene and make visual comparison difficult. But one could notice the deviation of CP-6H and CP-01, which could be candidates to be withdrawn. To better visualize the difference between the trajectories, the distance between each trajectory and the reference data (NOAA's best track) was computed and shown in Figure 5.2.

Figure 5.2 - Errors (distance) between the trajectories



Source: Made by the author (2025).

It can be confirmed that CP-01 deviates significantly from the expected trajectory. Additionally, CP-6H offer limited discussion, as it is quite similar to the other experiments within their group. In Figure 5.2 (d), CP-1HD05015km does not show a significant improvement and will consequently be withdrawn. We will retain CP-1HD050 to seek the effects related to this configuration in the context of other aspects of tropical cyclones.

To summarize the experiments we intend to keep, a new table has been created, similar to Table 5.1.

Table 5.4 - Selected Experiments

| Experiment | Description | ID |
|---------------------------|--|---|
| Cold Pool Effect | Turn on and off the cold pool parameterization scheme | CP-ON |
| | | CP-OFF (Control) |
| Initial Condition | Compares the effect of two initial conditions, June 29, July 2nd (noon), and July 3rd. Tested with 1st July. | CP-29 |
| | | CP-02T12 |
| | | CP-03 (Control) |
| Cold Pool Lifetime | Compares the effect of cold pool lifetime being 1h, 2h (default), 3h, and 6h | CP-1H |
| | | CP-2H (Control) |
| | | CP-3H |
| Maximum Down-draft Height | Compares the effect of the maximum downdraft height, being 0.25, 0.35, and 0.50 | CP-D025 |
| | | CP-D035 (Control) |
| | | CP-D050 |
| Resolution Experiment | Evaluates the resolution effect on the results, degrading it into 60 km and enhancing it into 15 km | CP-15km CP-30km (Control) CP-60km |
| Type of Initial Condition | Changes the type of initial condition to be from the GFS model | CP-ERA5 (Control) CP-GFS |
| Best Configuration Test | A run with two changes inside the cold pool parameters | CP-1HD050 |

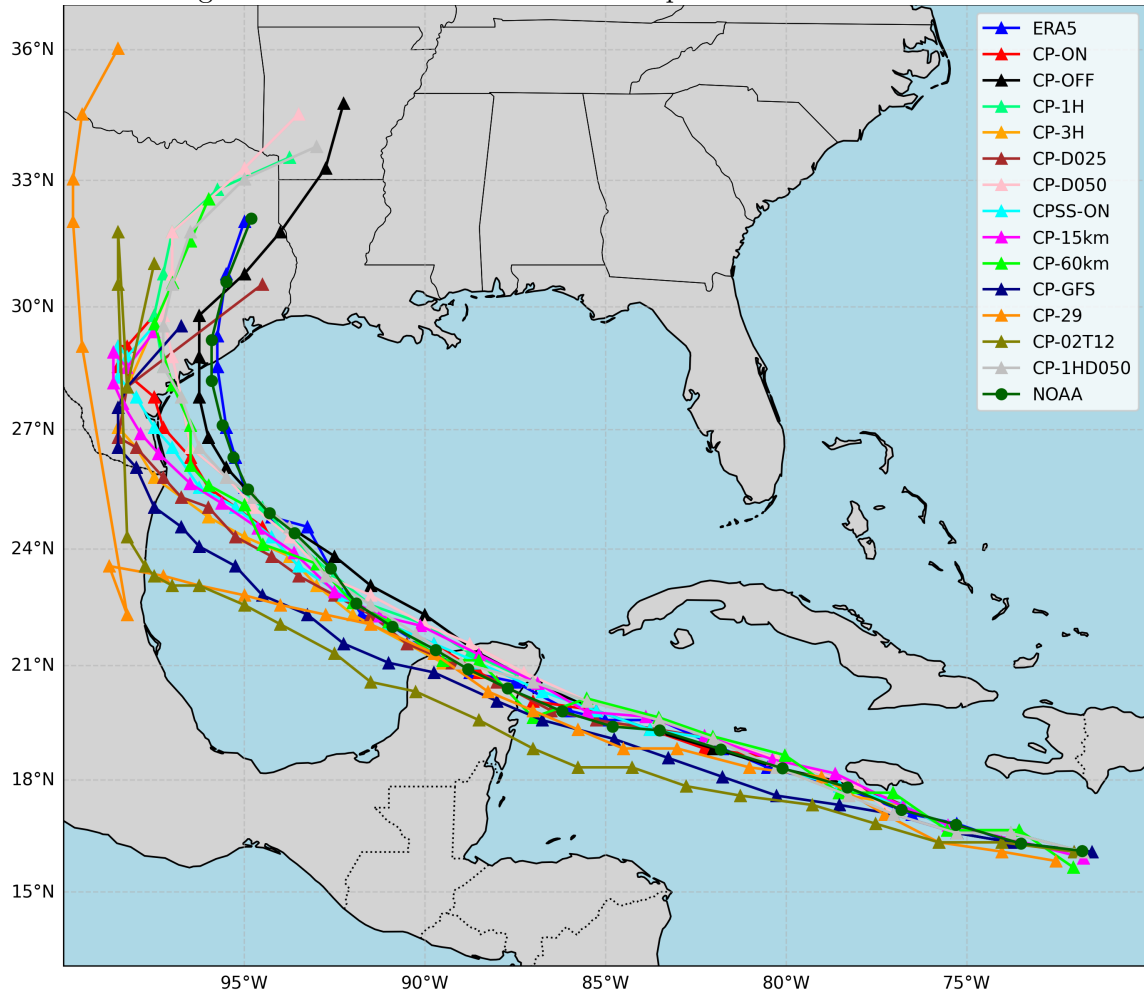
Source: Made by the author, 2025.

In the following subsection we will continue the results now keeping in mind the experiments listed at Table 5.4.

5.2.1 Trajectory

All trajectories are displayed in the Figure 5.3. The trajectories of each group of the Table 5.4 can be found at Appendix () .

Figure 5.3 - All tracks with selected experiments from Table 5.4



Source: Made by the author (2025).

5.2.2 Intensity

5.2.3 Rainfall

5.2.3.1 Pattern and spatial rainfall distribution

5.2.3.2 Rainfall mean and overall distribution

5.2.3.3 MONAN performance at forecasting rainfall

5.2.4 Discussion of key outcomes

6 CASE STUDY: HURRICANE HELENE – TESTING THE IMPROVED PARAMETRIZATION

6.1 Event description - Helene

6.2 Results and analysis of hurricane Helene

6.2.1 Trajectory

6.2.2 Intensity

6.2.3 Rainfall

6.2.3.1 Pattern and spatial rainfall distribution

6.2.3.2 Rainfall mean and overall distribution

6.2.3.3 MONAN performance at forecasting rainfall

6.3 Discussion of key outcomes

7 CONCLUSIONS AND FUTURE WORK

7.1 Future Work

A APPENDIX - THE MASS FLUX DEDUCTION

Here is briefly described the mass flux approach in the cold pool parameterization context.

A APPENDIX B - THE TRACKING ALGORITHM

Descrever o algoritmo assim como referencias.

REFERENCES

- BAGTASA, G. Assessment of tropical cyclone rainfall from gsmap and gpm products and their application to analog forecasting in the philippines. **Atmosphere**, MDPI, v. 13, n. 9, p. 1398, 2022. 9
- BOPAPE, M.-J. M.; CARDOSO, H.; PLANT, R. S.; PHADULI, E.; CHIKOORE, H.; NDARANA, T.; KHALAU, L.; RAKATE, E. Sensitivity of tropical cyclone idai simulations to cumulus parametrization schemes. **Atmosphere**, MDPI, v. 12, n. 8, p. 932, 2021. 5, 13
- DEMARIA, M.; KNAFF, J.; SAMPSON, C. Evaluation of long-term trends in tropical cyclone intensity forecasts. **Meteorology and Atmospheric Physics**, Springer, v. 97, n. 1, p. 19–28, 2007. 16
- DESHPANDE, M.; PATTNAIK, S.; SALVEKAR, P. Impact of physical parameterization schemes on numerical simulation of super cyclone gonu. **Natural Hazards**, Springer, v. 55, p. 211–231, 2010. 13
- DITCHEK, S. D.; SIPPEL, J. A.; MARINESCU, P. J.; JR, G. J. A. Improving best track verification of tropical cyclones: A new metric to identify forecast consistency. **Weather and Forecasting**, v. 38, n. 6, p. 817–831, 2023. 14
- DULAC, W.; CATTIAUX, J.; CHAUVIN, F.; BOURDIN, S.; FROMANG, S. Assessing the representation of tropical cyclones in era5 with the cnrm tracker. **Climate Dynamics**, Springer, v. 62, n. 1, p. 223–238, 2024. 5, 6
- FREITAS, S. R.; GRELL, G. A.; CHOVERT, A. D.; DIAS, M. A. F. S.; NASCIMENTO, E. de L. A parameterization for cloud organization and propagation by evaporation-driven cold pool edges. **Journal of Advances in Modeling Earth Systems**, Wiley Online Library, v. 16, n. 1, p. e2023MS003982, 2024. 1
- GAO, K.; HARRIS, L.; BENDER, M.; CHEN, J.-H.; ZHOU, L.; KNUTSON, T. Regulating fine-scale resolved convection in high-resolution models for better hurricane track prediction. **Geophysical Research Letters**, Wiley Online Library, v. 50, n. 13, p. e2023GL103329, 2023. 15
- HEMING, J. Tropical cyclone tracking and verification techniques for met office numerical weather prediction models. **Meteorological Applications**, Wiley Online Library, v. 24, n. 1, p. 1–8, 2017. 16
- HERSBACH, H.; BELL, B.; BERRISFORD, P.; HIRAHARA, S.; HORÁNYI, A.; MUÑOZ-SABATER, J.; NICOLAS, J.; PEUBEY, C.; RADU, R.; SCHEPERS, D. et al. The era5 global reanalysis. **Quarterly journal of the royal meteorological society**, Wiley Online Library, v. 146, n. 730, p. 1999–2049, 2020. 5
- HUFFMAN, G. Gpm imerg final precipitation l3 half hourly 0.1 degree× 0.1 degree v06. (**No Title**), 2019. 7
- JANOWIAK, J.; JOYCE, B.; XIE, P. **NCEP/CPC L3 half hourly 4 km global (60S–60N) merged IR V1. Goddard Earth Sciences Data and Information Services Center (GES DISC)**. 2017. 8

- KNAPP, K. R.; KRUK, M. C.; LEVINSON, D. H.; DIAMOND, H. J.; NEUMANN, C. J. The international best track archive for climate stewardship (ibtracs) unifying tropical cyclone data. **Bulletin of the American Meteorological Society**, American Meteorological Society, v. 91, n. 3, p. 363–376, 2010. 5
- LANDSEA, C. W.; FRANKLIN, J. L. Atlantic hurricane database uncertainty and presentation of a new database format. **Monthly Weather Review**, v. 141, n. 10, p. 3576–3592, 2013. 16
- MARCHOK, T.; ROGERS, R.; TULEYA, R. Validation schemes for tropical cyclone quantitative precipitation forecasts: Evaluation of operational models for us landfalling cases. **Weather and forecasting**, v. 22, n. 4, p. 726–746, 2007. 17, 18
- MAY, J.; HARANDI, M.; TYO, J. S.; HU, L.; RITCHIE-TYO, E. A. A cnn system for segmenting tropical cyclones neighborhoods in geostationary images. In: IEEE. **IGARSS 2024-2024 IEEE International Geoscience and Remote Sensing Symposium**. [S.l.], 2024. p. 8259–8262. 5
- MESINGER, F. Bias adjusted precipitation threat scores. **Advances in Geosciences**, Copernicus Publications Göttingen, Germany, v. 16, p. 137–142, 2008. 17
- MISHRA, A. K.; JANGIR, B.; KHAIN, P.; STROBACH, E. Characteristics of the mediterranean cyclone ianos in convection-permitting simulations: Unraveling model sensitivity to microphysics and cumulus parameterization. **Journal of Geophysical Research: Atmospheres**, Wiley Online Library, v. 129, n. 23, p. e2024JD041637, 2024. 13
- MOON, J.; PARK, J.; CHA, D.-H.; MOON, Y. Five-day track forecast skills of wrf model for the western north pacific tropical cyclones. **Weather and Forecasting**, v. 36, n. 4, p. 1491–1503, 2021. 14
- NYONGESA, A. M.; SHI, D.; LI, S.; LI, Q. Influence of convective parameterization on the simulation of tropical cyclones over the south west indian ocean: A case study of tropical cyclone idai (2019). **Atmospheric Research**, Elsevier, v. 306, p. 107461, 2024. 13, 14
- REDDY, M. V.; MITRA, A. K.; MOMIN, I.; KRISHNA, U. M. How accurately satellite precipitation products capture the tropical cyclone rainfall? **Journal of the Indian Society of Remote Sensing**, Springer, v. 50, n. 10, p. 1871–1884, 2022. 9
- SHEPHERD, T. J.; WALSH, K. J. Sensitivity of hurricane track to cumulus parameterization schemes in the wrf model for three intense tropical cyclones: Impact of convective asymmetry. **Meteorology and Atmospheric Physics**, Springer, v. 129, p. 345–374, 2017. 16
- YANG, S.; SURRATT, M.; WHITCOMB, T. R.; CAMACHO, C. Evaluation of imerg and gsmap for tropical cyclone applications. **Geophysical Research Letters**, Wiley Online Library, v. 51, n. 4, p. e2023GL106414, 2024. 5, 9
- ZARZYCKI, C. M.; ULLRICH, P. A.; REED, K. A. Metrics for evaluating tropical cyclones in climate data. **Journal of Applied Meteorology and Climatology**, v. 60, n. 5, p. 643–660, 2021. 13

ZHOU, Y.; MATYAS, C. J. Regionalization of precipitation associated with tropical cyclones using spatial metrics and satellite precipitation. **GIScience & Remote Sensing**, Taylor & Francis, v. 58, n. 4, p. 542–561, 2021. 5